Single-drive push-pull silicon Mach-Zehnder modulator for OOK and BPSK modulation

Haike Zhu[1], Linjie Zhou[1,*], Lei Liu[2], Tao Wang[2], Yanyang Zhou[1], Jinting Wang[1], Qianqian Wu[1], Anbang Xie[1],
Rui Yang[1], Zuxiang Li[1], Xinwan Li[1], and Jianping Chen[1]
[1]State Key Laboratory of Advanced Optical Communication Systems and Networks,
Department of Electronic Engineering, Shanghai Jiao Tong University, Shanghai 200240, P. R. China
[2]Transmission Technology Research Department, Huawei Technologies Co.Ltd.,
Shenzhen 518129, P.R. China
[*]ljzhou@sjtu.edu.cn

Paper Summary

We demonstrate a single-drive high-speed silicon Mach-Zehnder modulator with the $V_{\pi}{\cdot}L$ of 1.35 V·cm. 20 Gb/s on-off keying (OOK) and 15 Gb/s binary phase shift keying (BPSK) modulations are achieved.

Introduction

Silicon modulators have been well developed as key enabling devices in silicon photonics integrated chips. In general, silicon modulators demonstrated in the literature are made of two types of structures. One is the resonance structure such as microring resonators [1], which can achieve an on-off keying (OOK) modulation of over 40 Gb/s with a small footprint and low power consumption. However resonance structures are quite sensitive to temperature, limiting their practical use. The other one is the Mach-Zehnder Interferometer (MZI) structure. It is more tolerant to temperature variation but at the cost of a relatively large footprint. Mach-Zehnder modulators (MZM) can also achieve OOK modulation up to 40 Gb/s [2]. The insertion loss and power consumption have been greatly reduced by optimizing the *p-n* junction, particularily, its doping concentration and profile [3, 4].

Recently, binary phase shift keying (BPSK) modulation based on a silicon MZM has been studied [5], and shown to have an excellent chirp-free performance [6]. These devices are designed to have separate traveling wave electrodes (TWEs) on the two MZI arms, which have to be driven by differential radio-frequency (RF) signals.

In this paper, we experimentally demonstrate a silicon MZM with a single-drive push-pull traveling wave electrode. Benefiting from the compact electrode design, the device footprint is reduced and only one RF signal is needed to drive the modulator.

Device structure

Fig. 1(a) shows the confocal laser scanning microscope image of our silicon MZM. The MZI is composed of two 1×2 Multimode interference (MMI) couplers. The length difference between the MZI arms is 120 μm. The TWE driving the two series *p-n* junctions is 3 mm long. Fig. 1(b) shows the cross-sectional view of the silicon MZM. The waveguide dimension is 500 nm × 220 nm with a slab height of 60 nm. The lateral p-n junction has a 100 nm offset towards *n* doping region. The doping concentrations are 4×10^{17} cm^{-3} and 1×10^{18} cm^{-3} for the *p* and *n* doping regions, respectively. The n^+ doping region is in the center of the MZI with a doping concentration of ~10^{20} cm^{-3} for ohmic contract with the DC bias metal line, as shown in Fig. 1(a). Two p^+ doping regions are placed outside the Mach-Zehnder arms with a doping concentration of ~10^{20} cm^{-3}. They connect to the signal and ground lines of the TWE.

Figs. 1(c) and 1(d) show the simulated free-carrier distributions in the arm waveguides at 0 V and -5 V, respectively. The depletion region increases from ~80 nm to ~250 nm when the applied voltage changes from 0 V to -5 V, leading to an effective refraction index change of 2.77×10^{-4} and phase change of 1.07π due to the free-carrier plasma dispersion effect. Therefore, the modulation efficiency is $V_{\pi}{\cdot}L$ = ~1.5 V·cm.

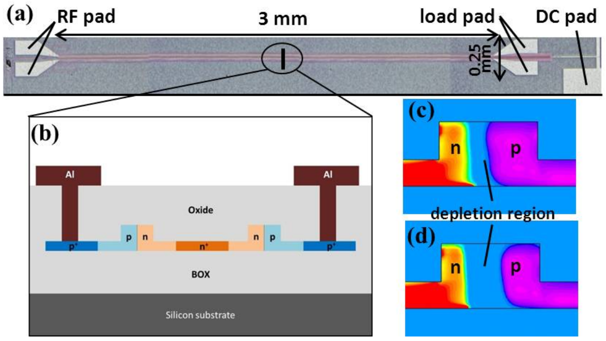

Fig. 1. (a) Microscope image of the silicon MZM. (b) Cross-sectional view of the silicon MZM with a single-drive push-pull electrode design. (c) and (d) Simulated free-carrier distributions in the MZI arm waveguides at (c) 0 V and (d) -5 V.

Experimental results

We used a tunable laser as the light source. The input light was transverse-electrically (TE) polarized by using a polarize controller. Light was coupled into the waveguide using a lensed fiber. The fiber to fiber insertion loss is ~25 dB, including ~8 dB coupling loss per facet, ~1 dB loss per MMI coupler, and ~7 dB loss from modulation arms due to junction doping. It should be noted that MMI couplers can be optimized to have <0.1 dB loss [7]. Fig. 2(a) shows the measured transmission spectra of the silicon MZM in one free spectrum range (FSR) when the upper arm is biased from 0 V to -5 V. At 0 V, null tranmission (due to destructive interference) occurs at 1541.8 nm with an extinction ratio (ER) of ~25 dB. The ER decreases to 15 dB as the reverse bias increases due to the unbalanced arm loss. The average wavelength shift is 0.5 nm/V, which is very sensitive to reverse bias due to the relatively high doping concentration of the *p*-*n* junction. The π-phase shift is achieved around -4.5 V. Therefore, the measured $V_{\pi}\cdot L$ is 1.35 V·cm, consistent with the simulation result. Fig. 2(b) shows the electro-electro (EE) S_{21} response of the TWE measured by a vector network analyzer (VNA). The S_{21} parameter reflects the RF signal transmission loss. The 6-dB bandwidth is 12.6 GHz at 0 V and rises up to 21.5 GHz at -5 V. The bandwidth improvement with the increasing reverse bias is resulted from the reduction of *p*-*n* junction capacitance. From the simulated frequency responses of RF loss, RF and optical effective refractive indices, and TWE characteristic impedance, we deduce the electro-optical (EO) bandwidth is around 28 GHz at -5 V.

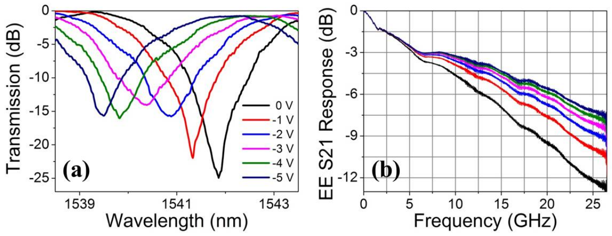

Fig. 2. (a) Optical transmission spectra of our silicon MZM at various bias voltages. (b) EE S_{21} responses of the TWE.

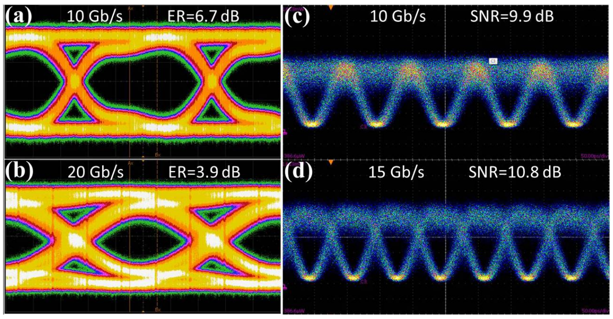

Fig. 3. (a) and (b) Measured OOK eye diagrams at 10 Gb/s and 20 Gb/s. (c) and (d) Measured BPSK eye diagrams at 10 Gb/s and 15 Gb/s.

We first measured the eye diagrams of the modulated OOK optical signals. The 2^{31}-1 pseudo-random binary sequence (PRBS) RF signal was generated from a pulse pattern generator (PPG) and amplified to 7 V (peak-to-peak) by an RF amplifier. The RF signal was applied onto the MZM via a 40 GHz microwave probe. The end of the TWE was terminated with a 50-ohm resistor using another microwave probe. The modulated optical signal from the MZM was amplified by an erbium-doped optical fiber amplifier (EDFA) to compensate for the modulator insertion loss. A 1-nm bandwidth optical filter was used to suppress the ASE noise before the modulated optical sigal detected by a 100 GHz bandwidth photodetector. The electrical signal was finally sent to a digital signal analyzer (DSA). The DC bias was -4 V while the wavelength was set at the quadrature point of the MZI around 1541.2 nm. The 10 Gb/s OOK eye diagram is shown in Fig. 3(a) with a Q-factor of 7.8 and an ER of 6.7 dB. The 20 Gb/s OOK eye diagram is shown in Fig. 3(b) with a Q-factor of 5.4 and an ER of 3.9 dB.

We next measured the eye diagrams of the BPSK optical signals. The modulated optical signal was sent to an optical oscilloscope integrated with a low noise amplifier (LNA). The DC bias was set at -5 V and the wavelength was tuned to 1539.5 nm. The 10 Gb/s BPSK eye diagram is shown in Fig. 3(c) with a signal-to-noise ratio (SNR) of 9.9 dB. The 15 Gb/s BPSK eye diagram is shown in Fig. 3(d) with a SNR of 10.8 dB. The characteristic impedance of the TWE is around 60 ohm obtained from simulation. The power consumption can thus be estimated as $P=\frac{1}{4}\cdot\frac{V_{pp}^{2}}{R}=\sim 204$ mW ($V_{pp}=7$ V, $R=60\ \Omega$) [8], corresponding to 13.5 pJ/bit for the 15 Gb/s BPSK modulation.

Conclusions

We experimentally demonstrated a 3 mm long silicon MZM with a single-drive push-pull TWE. The measured $V_{\pi}\cdot L$ is ~1.35 V·cm. The 6-dB EE bandwidth of the TWE is 21.5 GHz at -5 V. Preliminary measurements show that our modulator can realize 20 Gb/s OOK and 15 Gb/s BPSK modulation. The modulation rate could be further improved by optimizing the TWE design to reduce its microwave loss.

References

1. T. Baba et al, *Optics Express* 21 (2013) p. 11869-76
2. M. Ziebell et al, *Optics Express* 20 (2012) p. 10591-6
3. X. Xiao et al, *Optics Express* 21 (2013) p. 4116-25
4. M. Streshinsky et al, *Optics Express* 21 (2013) p. 23410-5
5. T. Li et al, *Optics Express* 21 (2013) p. 23410-5
6. K. Goi et al, OECC (2012) p. 238-239
7. S. Zhen et al, *IEEE Photonics Journal* 4 (2012) p. 2272-2277
8. J. Ding et al, *Optics Express* 20 (2012) p. 7081-7